Comparing source inversion techniques for GPS-based local tsunami forecasting: A case study for the April 2014 *M*8.1 Iquique, Chile, earthquake

Kejie Chen[1], Andrey Babeyko[1], Andreas Hoechner[1], and Maorong Ge[1]

[1]German Research Centre for Geosciences, Potsdam, Germany

Abstract Real-time GPS is nowadays considered as a valuable component of next generation near-field tsunami early warning systems able to provide fast and reliable source parameters. Looking for optimal methodologies and assessing corresponding uncertainties becomes an important task. We take the opportunity and consider the 2014 Pisagua event as a case study to explore tsunami forecast uncertainty related to the GPS-based source inversion. We intentionally neglect all other sources of uncertainty (observation set, signal processing, wave simulation, etc.) and exclusively assess the effect of inversion technique. In particular, we compare three end-member methods: (1) point-source fastCMT (centroid moment tensor), (2) distributed slip along predefined plate interface, and (3) unconstrained inversion into a single uniform slip finite fault. The three methods provide significantly different far-field tsunami forecast but show surprisingly similar tsunami predictions in the near field.

1. Introduction

In aftermath of the 2004 Sumatra tragedy and in response to the need in more reliable near-field tsunami early warning systems (TEWS), researchers proposed continuous real-time GPS arrays for fast and enhanced tsunami source inversion [see, e.g., *Blewitt et al.*, 2006; *Sobolev et al.*, 2006, 2007; *Song*, 2007]. The idea of using real-time GPS for TEWS is clear: for large tsunami-triggering seismic events, traditional broadband instruments near the source may saturate, and thus, the magnitude estimation relies on teleseismic waves recorded much later at distant stations which inevitably delays early warning. Alternatively, local GPS networks with real-time processing are able to provide ground displacements without saturation almost without delay: a trustworthy tool for near-field earthquake characterization and tsunami early warning [*Ohta et al.*, 2012; *Hoechner et al.*, 2013; *Li et al.*, 2013b]. In parallel, methods based on traditional seismic instrumentation also developed toward faster source solution. *Kanamori and Rivera* [2008] introduced source inversion based on the long-period *W* phase, a *P* wave precursor to large-amplitude *S* and surface waves. Recently, validity of this method was tested in the near field by retrospective analysis of the 2011 Tohoku-Oki event [*Gusman and Tanioka*, 2014]. The authors concluded that *W* phase inversion using only 5 min long data record can provide solution sufficiently accurate for tsunami early warning purposes. To address the problem of broadband clipping, seismic stations in the near field can be also are augmented with strong-motion recorders. The latter, however, require a double integration to convert accelerations into displacements, which may become unreliable at low frequencies because tilts of the instruments are indistinguishable from translations, and any errors are amplified in the integration [*Bock et al.*, 2011; *Li et al.*, 2013a]. Subjective correction algorithms are available but require the full waveform, and the permanent deformation that accompanies large earthquakes may be filtered out or not estimated correctly in this process [*Melgar et al.*, 2013a]. One solution to this problem is, again, incorporation of real-time GPS sensors, which gave an impulse to the new technique of combined processing of strong-motion and GPS records: "seismogeodesy" [see, e.g., *Bock et al.*, 2011; *Tu et al.*, 2013].

In order to be used for tsunami early warning and forecasting, coseismic displacements captured by a coastal GPS network need to be inverted into source parameters (e.g., epicenter, magnitude, and slip distribution) on-the-fly to initialize tsunami scenarios. Actually, numerous previous studies have been focused on inversion methodologies. Recently, *Melgar et al.* [2012] proposed an algorithm called *fastCMT* to obtain centroid moment tensor (CMT) and location for earthquakes using local and regional real-time GPS coseismic displacements. Original fastCMT algorithm assumed point source inversion, and to account for the source finiteness, it was later extended to a linear geometry by superposition of point sources [*Melgar et al.*, 2013b].
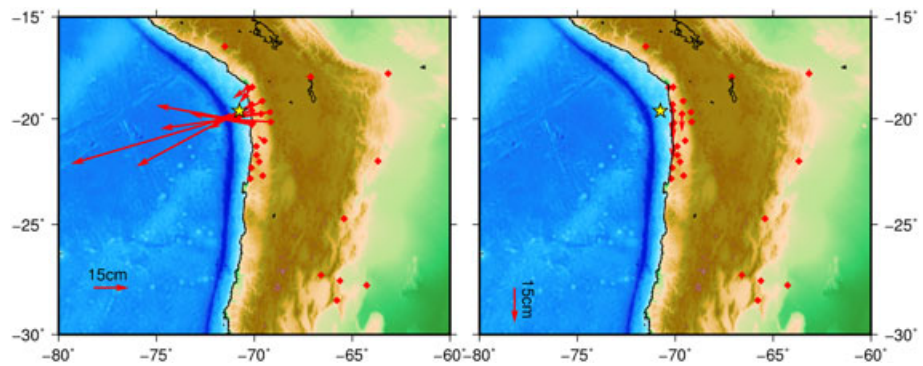
Figure 1. Coseismic offset from TPP. (left) Horizontal and (right) vertical displacements, while the yellow star shows the epicenter from U.S. Geological Survey.

Instead of adopting coseismic displacements, *O'Toole et al.* [2012] developed an algorithm to get centroid moment tensor using high-rate GPS waveforms. They also suggested an alternative to the fastCMT approach by simultaneously searching for the best centroid position [*O'Toole et al.*, 2013]. *Crowell et al.* [2012] inverted real-time GPS data for a finite fault slip distribution in homogeneous elastic half-space. In their method, a priori information on fault geometry can be either predefined or derived from the rapid CMT solution. Taking the 2011 Tohoku tsunami as an example, *Hoechner et al.* [2013] replayed the whole hypothetical GPS-based tsunami forecasting processing chain: starting from the real-time processing of raw GPS data down to on-the-fly tsunami simulations. The replay has demonstrated the feasibility of reliable GPS-based tsunami early warning in less than 3 min. Within this exercise, *Hoechner et al.* [2013] inverted coseismic GPS displacements into nonuniform slip distribution at a curved plate interface. *Ohta et al.* [2012] retrospectively inverted the 2011 Tohoku earthquake on a rectangular fault using uniform slip. In contrast with many other studies, their inversion algorithm does not fix the fault geometry and position a priori allowing the unconstrained inversion into finite fault parameters.

While a number of studies focused on tsunami source inversion using GPS data were published last years, no systematic study was undertaken to compare the inversion differences and, what is more important, to assess these differences in relation to the final tsunami forecasting. The north Chile, 1 April 2014, Iquique M8.1 earthquake and tsunami were extensively recorded by a large number of land- and ocean-based instruments [e.g., *Schurr et al.*, 2014]. In particular, significant coseismic displacements were recorded at several coastal GPS stations. In the present contribution, we take the opportunity and use the 2014 Iquique event as a case study to explore uncertainties of the GPS-based real-time tsunami forecasting related to different source inversion methods. Specifically, we compare three inversion methods: (1) point-source fastCMT [*Melgar et al.*, 2012], (2) inversion into slip distribution along the predefined curved plate interface, and (3) unconstrained inversion into a single finite fault with uniform slip. Of particular note, in contrast to megaearthquakes like the 2011 Tohoku M9.0 event which definitely cause devastating tsunamis, earthquakes like the 2014 Iquique event, with magnitudes ranging from M7.5 to M8.5 are especially challenging for TEWS because they belong to the "grey zone." On the one hand, they do not necessarily trigger tsunamis; on the other hand, GPS fingerprints of such earthquakes may also approach the limit of real-time detectability.

2. Retrieving Coseismic Offsets From Real-Time GPS Waveforms

In this paper, Temporal Point Positioning (TPP) developed by *Li et al.* [2013c] was employed to retrieve real-time coseismic offset from the GPS stations of the Integrated Plate Boundary Observatory Chile (IPOC) (http://www.ipoc-network.org). To simulate data processing in a real-time mode, real-time precise satellite orbits and clock products are required. In this contribution, we generated them by positioning and navigation data analyst software [*Liu and Ge*, 2003]; for detailed estimation strategy, please refer to *Fang et al.* [2013]. Station distribution of the continuous GPS network is depicted in Figure 1. Among these stations, 11 ones are recorded with 1 s sampling interval while others having 30 s sampling interval. With respect to data processing, the cutoff angle is set as 7°. For troposphere, dry and wet parts were calculated using model provided by *Saastamoinen* [1972]. Coseismic waveforms were retrieved through epoch solution, and static offsets were

Table 1. GPS-Based fastCMT Moment Tensor Solution for the April 2014, Iquique, Northern Chile M8.1 Earthquake (Left) as Compared to the Global CMT (GCMT) Teleseismic Solutions[a]

Plane	fastCMT[b]			GCMT[c]		
	Strike	Dip	Rake	Strike	Dip	Rake
NP1	9	38	126	355	15	106
NP2	146	60	65	159	76	86

[a]VR means variance reduction, and NP stands for nodal plane.
[b]Centroid: $-70.81°$, $-19.90°$, -34.9 km; $M_w = 8.2$, VR = 88.6.
[c]Centroid: $-70.81°$, $-19.70°$, -21.6 km; $M_w = 8.1$.

obtained by the approach suggested by *Allen and Ziv* [2011]. Retrieved coseismic offsets are shown in Figure 1.

3. Inverting Tsunami Source Using Different Methods

Inversion of coseismic displacements into tsunami source parameters precedes simulation of tsunami propagation and coastal forecasting. It can be done either by matching of precomputed scenarios [*Behrens et al.*, 2010] or by on-the-fly retrieving of a set of source parameters enabling initiation of tsunami propagation simulation. Sets of source parameters correspond to underlying rupture models and, hence, differ for different inversion methods. In present study we compare the three aforementioned inversion methods using coseismic displacements from section 2. Please note that taking into account the noise level of GPS displacements, only stations with coseismic offsets larger than 1.5 cm were included in the following inversions. In order to assess the effect of source inversion onto the final tsunami forecast, we have simulated tsunami generation and propagation for each inverted source model. *easyWave* [*Hoechner et al.*, 2013; http://trac.gfz-potsdam.de/easywave] code was used to calculate 4 h of tsunami propagation. The computational algorithm of easyWave follows the linear long-wave numerical scheme on a staggered spherical finite-difference grid with leapfrog explicit time stepping [*Goto et al.*, 1997]. Bathymetry was GEBCO 30 arc seconds grid (*The GEBCO_08 Grid, version 20100927*, http://www.gebco.net), and boundary conditions include normal reflections at the coastline plus radiation boundary conditions at open boundaries.

3.1. Result From fastCMT

In 2012, *Melgar et al.* [2012] proposed fastCMT: an effective MATLAB-based algorithm to convert GPS residual coseismic displacements into the central moment tensor parameters. Following Melgar's algorithm, we have computed moment tensor synthetic Green's functions using EDGRN code [*Wang et al.*, 2003] and AK135 seismic velocity model [*Kennett et al.*, 1995] with 2 km horizontal and 4 km vertical intervals. At station locations, Green's functions were evaluated by spline interpolation from the closest grid nodes. Since the original fastCMT algorithm best fits moment tensor parameters at fixed geographical location, it should be accomplished with a grid search routine to find the best fit centroid location as well. With respect to this search, we scanned within a 3-D $2° \times 2° \times 40$ km prism by nodes spaced 0.2° horizontal and 4 km by depth and centered on the rapid epicenter from triggering seismic message. In accord with real-time GPS precision, horizontal components were weighted twice as much as the vertical component.

Corresponding best fit fastCMT solution for the Iquique 2014 earthquake is summarized in Table 1. For reference, we compare it with the teleseismic Global CMT (GCMT) provided by the GCMT project (http://www.globalcmt.org/CMTsearch.html).

The fastCMT method provides source parameters in a point-source approximation. At the same time, tsunami initiation requires a finite fault model to calculate initial surface disturbance. To meet this requirement, we have extended CMT results and estimated corresponding fault length, width, and slip by applying scaling relations of *Blaser et al.* [2010] to the derived magnitude. Resulting parameter set (hypocenter, strike, dip, rake, fault length, width, and amount of slip) constitutes the input to the well-known *Okada* [1985] uniform slip rupture model routinely used in tsunami simulations. Of course, this procedure of transformation from point-source to a finite source does not guarantee the same quality of GPS fit by the both models. Figure 2a presents GPS inversion results with the fastCMT method and the corresponding finite fault model.

3.2. Result From Distributed Slip Inversion

Slip inversion along the predefined plane or curved subduction plate interface is nowadays a common strategy for GPS-based source inversions. In this study we use the inversion algorithm described in *Hoechner et al.* [2008, 2013]. Slab geometry follows the Slab1.0 subduction zones model by *Hayes et al.* [2012], and elastic model corresponds to layered half-space. Figure 2b presents the final rupture model of the Iquique earthquake.
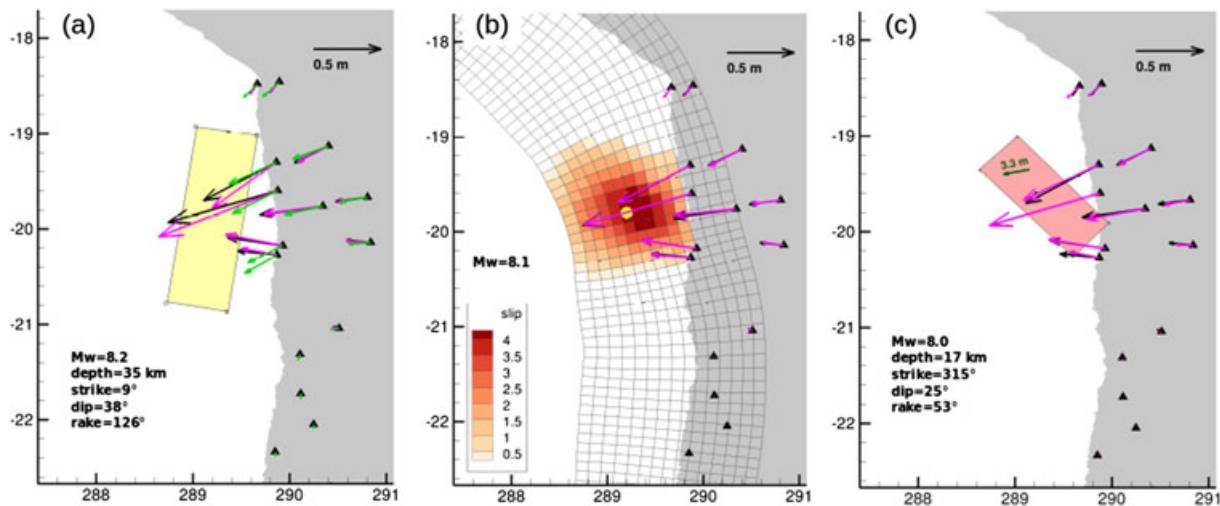
Figure 2. Source models for the April 2014 Iquique earthquake obtained by the three tested GPS inversion methods. (a) fastCMT method by *Melgar et al.* [2012]. Magenta vectors correspond to the best point-source fit. Note that the finite fault model (yellow rectangle) derived from the best fit CMT solution generates displacements (green) which fit observed GPS vectors (black) considerably worse. (b) Slip distribution along the predefined Slab1.0 curved plate interface. (c) Unconstrained inversion into a single uniform slip fault without any a priori information. Note that strike of the plane does not follow direction of the trench.

3.3. Result From Inversion Into Single Finite Fault With Uniform Slip

Inversion into slip distribution along the predefined plate interface produces best fit results for classical subduction zone thrust ruptures. However, and that is important to note in the context of tsunami early warning, a "classical" thrust rupture between the subducted and upper plate is not the only possible rupture type in the vicinity of subduction zones. Less common but still widespread are ruptures of another types originating apart of the plate interface: e.g., outer rise normal faults, interslab earthquakes, and events in the upper plate. For a TEWS it is hence important not to treat all events as interslab thrusts by default (despite the latter often may be considered as worst case scenario) but to be able to invert source without any prejudgement on focal mechanism and orientation. To meet this requirement, we have also included into the present study unconstrained inversion into a single finite fault with minimal a priori information. The only constraint we used was the scaling law by *Blaser et al.* [2010] linking fault size and slip to the earthquake magnitude. Independent search parameter set included: epicenter, depth, magnitude, strike, dip, and rake angles. Parameter space search for the best fit was organized as a combination of brute force and Monte Carlo searches. No precomputed Green's functions were used in the inversion procedure; instead, trial displacements at GPS stations were computed each time using the *Okada* [1985] formulas. Figure 2c shows the best fit fault model. Note that due to the trade-off between the strike and rake angles, the strike of the best fit model does not follow the actual trench direction.

3.4. Tsunami Forecasts From Different Source Inversions

The main goal of the current study is to assess the uncertainty of tsunami forecasting related to different source inversion techniques. Figures 3 and 4 display the results of tsunami propagation scenarios corresponding to the three aforementioned source inversions. Figure 3 presents the distribution of maximum wave heights at a regional scale. The three different source models produce significantly different wave radiation patterns that would result in different far-field tsunami forecasting (compare Figures 3a–3c). However, closer inspection of Figure 4 showing distribution of peak tsunami amplitudes along the nearby Chilean coast reveals almost opposite result: in the context of local tsunami early warning, the three source inversions would have produced similar coastal forecasting. That is because tsunami early warning centers, operating with simulation-based forecasts, usually assign warning levels ("advisory," "watch," "warning," and "major warning") to wave height thresholds. For example, if we accept 0.5 m as a warning threshold, we would rise the warning alert for the Chilean coast starting from 16.5°S down to 23.5°S for the all three models. Of course, predicted wave heights can exhibit significant differences at individual locations between the three source models. For example, absolute maximums of coastal tsunami amplitudes vary from 4 (Figure 4b) to 6 m (Figure 4c). Also, the overall
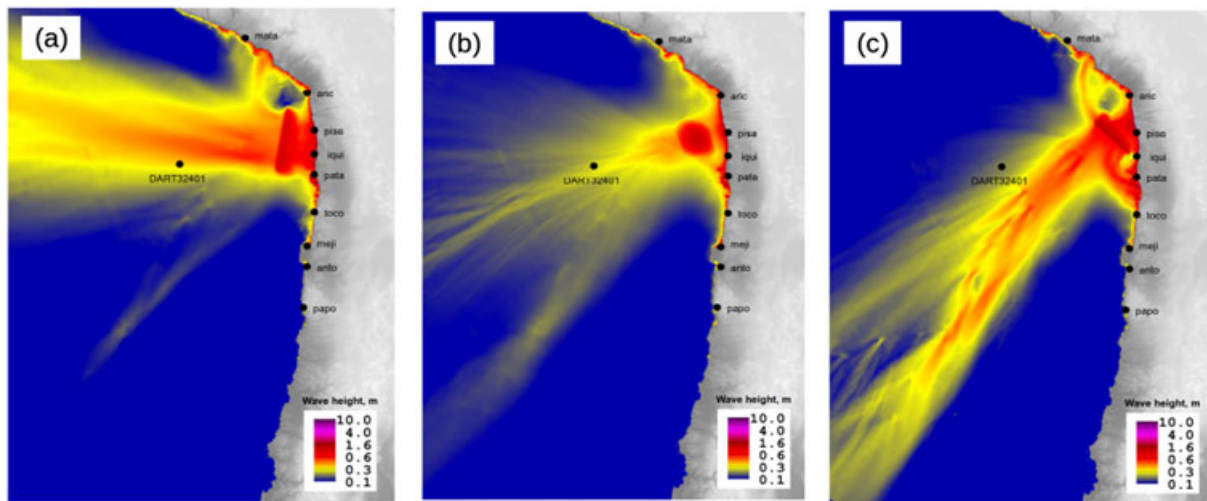
Figure 3. Maximum tsunami wave heights after 4 h of simulation for (a–c) the three different source invertion models. See Figure 2 and text for description of models in Figures 3a–3c.

amplitude pattern for the fastCMT source model is shifted to the north compared to another source models. But all these differences take place above the 0.5 m threshold and, therefore, become not important when a warning center evaluates its tsunami early warning forecast based on thresholds.

4. Concluding Remarks

We have used GPS data recorded by the IPOC network during the April 2014 Iquique, northern Chile M8.1 earthquake to assess tsunami forecast uncertainty related to different GPS-based source inversion methods. Three methods were compared: (1) point-source fastCMT with subsequent construction of uniform slip finite fault, (2) inversion into slip distribution along the predefined curved plate interface, and (3) unconstrained inversion into a single finite fault with uniform slip. These three methods are not unique; there are numerous variations of these techniques (see, for example, citations in section 1). However, the above algorithms effectively represent end-members of source inversion from static GPS displacements. Each of them is capable to work in real time and thus is suitable for early warning applications. Time cost for the first and second approach lies within several seconds on common workstation. Preliminary implementation of the unconstrained inversion by combination of brute force and Monte Carlo searches is not yet ready for operational use; draft inversion procedure takes several minutes. However, operative implementation has enormous optimization potential, first of all in parallelization and better guided search.

The three source inversion approaches give similar first-order rupture parameters including magnitude and longitude-latitude position of the rupture center. Other fault parameters: depth, strike, dip, and rake angles show significant differences, which are later clearly manifested by different far-field tsunami propagation patterns.

Despite large differences in far-field tsunami propagation (Figure 4), early warning tsunami forecasting along the nearby Chilean coast would be surprisingly similar for all three models (Figure 3). That is valid in case early warning alert is based on tsunami amplitude thresholds (e.g., 0.5 m threshold). In this case, even remarkable differences at individual locations do not change the alert status as long as they lie above the alert threshold. Our study does not reveal any absolute favorite between the three source inversion approaches.

It is important to note that the present result on robustness of the local tsunami early warning forecasting against source inversion technique should not be blindly projected to other subduction zones or to larger magnitudes. The 2014 Iquique 2014 M8.1 rupture was rather compact (<200 km) with simple, centered slip distribution. In a hypothetical case of a longer rupture (e.g., like Sumatra 2004), local irregularities of slip distribution might strongly influence runup distribution along the nearby coast [*Geist*, 2001]. Also, *Sobolev et al.* [2007] argued on extreme sensitivity of local runup against rupture position and slip distribution for the Sumatran west coast, Indonesia. In the latter case, high sensitivity to source parameters was due to specific
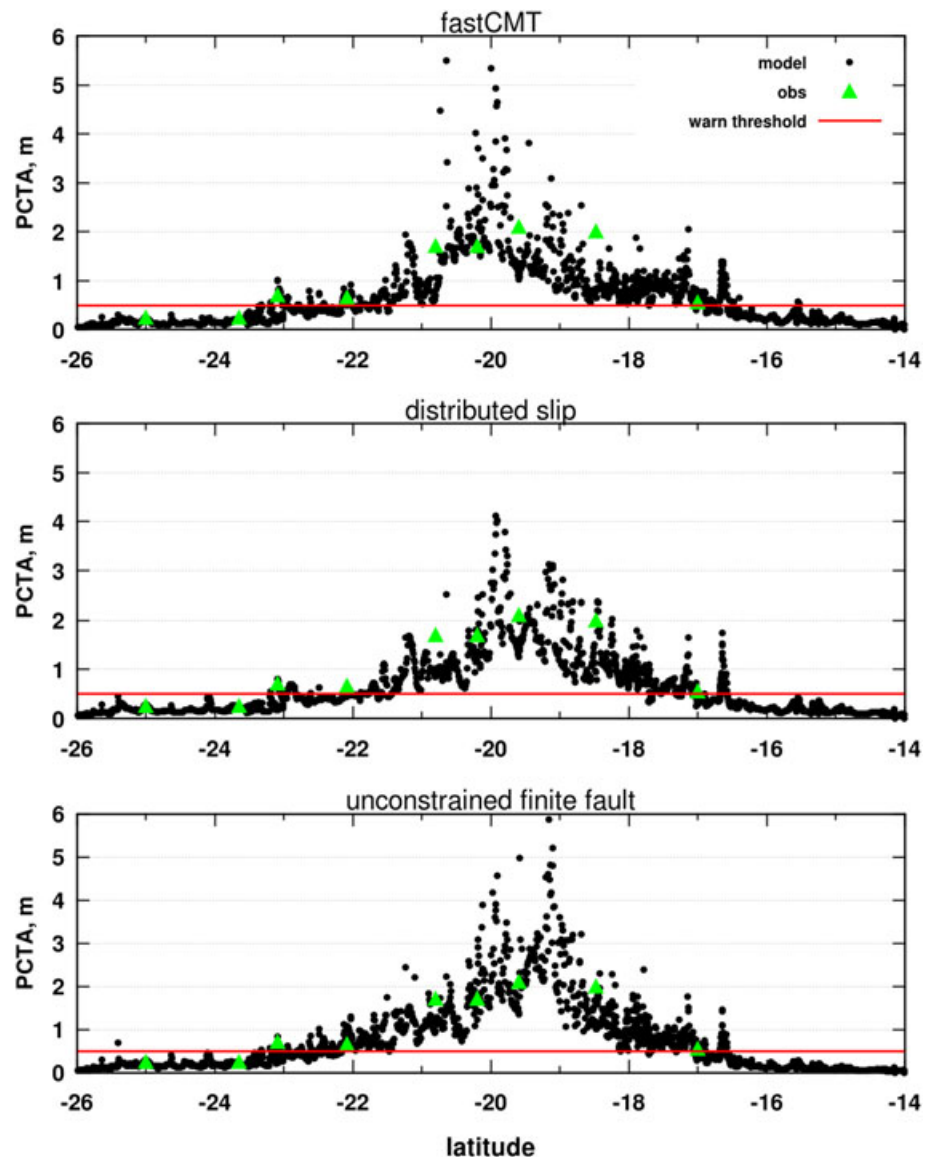
Figure 4. Peak tsunami amplitudes along the Chilean coast (dots) as forecasted for the three different source inversion models (see caption of Figure 2 for the model descriptions). Also shown are tsunami observations at the tide gauge stations (green triangle, raw data available from www.ioc-sealevelmonitoring.org). Horizontal red line represents the virtual warning level threshold. Note that "alerted" areas are very similar for the three models: from approximately 16.5°S to 23.5°S.

bathymetry offshore Sumatra—the presence of irregular Mentawai island chain. Regional and national near-field TEWS should build their own source inversion strategies based on corresponding tectonic settings.

Finally, it is important to note that in present study we have explored only one single source of forecast uncertainty: GPS-based source inversion algorithms. For that, we intentionally neglected all other sources of uncertainty related to, e.g., observation set and signal processing, wave simulation. In reality, operational tsunami forecasting deals with many sources of uncertainty: epistemic and aleatoric, related to data and to numerical methods. It is important to assess and to rank at least major sources of uncertainties in a systematic way for a more reliable tsunami early warning.

As revision of this manuscript was in progress, a new comprehensive study on perspectives of local tsunami warning with land-based GPS and strong-motion sensors was published by *Melgar et al.* [2016]. The two studies independently demonstrate the robustness of the local tsunami warning using fast source models from local land-based observations. In comparison to *Melgar et al.* [2016], our study explicitly addresses forecast

uncertainty due to the one selected component of the early warning chain—source inversion technique for static GPS displacements. Additionally, we demonstrate that while providing fairly similar (and reliable) local forecasts, fast source models may result in highly variable and less confident far-field forecasting.

References

Allen, R. M., and A. Ziv (2011), Application of real-time GPS to earthquake early warning, *Geophys. Res. Lett.*, *38*, L16310, doi:10.1029/2011GL047947.

Behrens, J., A. Androsov, A. Y. Babeyko, S. Harig, F. Klaschka, and L. Mentrup (2010), A new multi-sensor approach to simulation assisted tsunami early warning, *Nat. Hazards Earth Syst. Sci.*, *10*, 1085–1100, doi:10.5194/nhess-10-1085-2010.

Blaser, L., F. Kruger, M. Ohrnberger, and F. Scherbaum (2010), Scaling relations of earthquake source parameter estimates with special focus on subduction environment, *Bull. Seismol. Soc. Am.*, *100*(6), 2914–2926, doi:10.1785/0120100111.

Blewitt, G., C. Kreemer, W. C. Hammond, H.-P. Plag, S. Stein, and E. Okal (2006), Rapid determination of earthquake magnitude using GPS for tsunami warning systems, *Geophys. Res. Lett.*, *33*, L11309, doi:10.1029/2006GL026145.

Bock, Y., D. Melgar, and B. W. Crowell (2011), Real-time strong-motion broadband displacements from collocated GPS and accelerometers, *Bull. Seismol. Soc. Am.*, *101*(6), 2904–2925, doi:10.1785/0120110007.

Crowell, B. W., Y. Bock, and D. Melgar (2012), Real-time inversion of GPS data for finite fault modeling and rapid hazard assessment, *Geophys. Res. Lett.*, *39*, L09305, doi:10.1029/2012GL051318.

Fang, R., C. Shi, W. Song, G. Wang, and J. Liu (2013), Determination of earthquake magnitude using GPS displacement waveforms from real-time precise point positioning, *Geophys. J. Int.*, doi:10.1093/gji/ggt378.

Geist, E. L. (2001), Effect of depth-dependent shear modulus on tsunami generation along subduction zones, *Geophys, Res. Lett.*, *28*(7), 1315–1318, doi:10.1029/2000GL012385.

Goto, C., Y. Ogawa, N. Shuto, and F. Imamura (1997), *IUGG/IOC Time Project, Numerical Method of Tsunami Simulation with the Leap-Frog Scheme, IOC Manuals and Guides*, 35, Paris.

Gusman, A. R., and Y. Tanioka (2014), W phase inversion and tsunami inundation modeling for tsunami early warning: Case study for the 2011 Tohoku event, *Pure Appl. Geophys.*, *171*(7), 1409–1422.

Hayes, G. P., D. J. Wald, and R. L. Johnson (2012), Slab1.0: A three-dimensional model of global subduction zone geometries, *J. Geophys. Res.*, *117*, B01302, doi:10.1029/2011JB008524.

Hoechner, A., A. Y. Babeyko, and S. V. Sobolev (2008), Enhanced GPS inversion technique applied to the 2004 Sumatra earthquake and tsunami, *Geophys. Res. Lett.*, *35*, L08310, doi:10.1029/2007GL033133.

Hoechner, A., M. Ge, A. Y. Babeyko, and S. V. Sobolev (2013), Instant tsunami early warning based on real-time GPS—Tohoku 2011 case study, *Nat. Hazards Earth Syst. Sci.*, *13*(5), 1285–1292, doi:10.5194/nhess-13-1285-2013.

Kanamori, H., and L. Rivera (2008), Source inversion of W phase: speeding up seismic tsunami warning, *Geophys. J. Int.*, *175*(1), 222–238, doi:10.1111/j.1365-246X.2008.03887.x.

Kennett, B. L. N., E. R. Engdahl, and R. Buland (1995), Constraints on seismic velocities in the Earth from traveltimes, *Geophys. J. Int.*, *122*(1), 108–124.

Li, X., M. Ge, Y. Zhang, R. Wang, B. Guo, J. Klotz, J. Wickert, and H. Schuh (2013a), High-rate coseismic displacements from tightly integrated processing of raw GPS and accelerometer data, *Geophys. J. Int.*, doi:10.1093/gji/ggt249.

Li, X., M. Ge, X. Zhang, Y. Zhang, B. Guo, R. Wang, J. Klotz, and J. Wickert (2013b), Real-time high-rate co-seismic displacement from ambiguity-fixed precise point positioning: Application to earthquake early warning, *Geophys. Res. Lett.*, *40*, 295–300, doi:10.1002/grl.50138.

Li, X., M. Ge, B. Guo, J. Wickert, and H. Schuh (2013c), Temporal point positioning approach for real-time GNSS seismology using a single receiver, *Geophys. Res. Lett.*, *40*, 5677–5682, doi:10.1002/2013GL057818.

Liu, J., and M. Ge (2003), PANDA software and its preliminary result of positioning and orbit determination, *Wuhan Univ. J. Nat. Sci.*, *8*(2), 603–609.

Melgar, D., Y. Bock, and B. W. Crowell (2012), Real-time centroid moment tensor determination for large earthquakes from local and regional displacement records, *Geophys. J. Int.*, *188*(2), 703–718, doi:10.1111/j.1365-246X.2011.05297.x.

Melgar, D., Y. Bock, D. Sanchez, and B. W. Crowell (2013a), On robust and reliable automated baseline corrections for strong motion seismology, *J. Geophys. Res. Solid Earth*, *118*, 1177–1187, doi:10.1002/jgrb.50135.

Melgar, D., B. W. Crowell, Y. Bock, and J. S. Haase (2013b), Rapid modeling of the 2011 M_w 9.0 Tohoku-oki earthquake with seismogeodesy, *Geophys. Res. Lett.*, *40*, 2963–2968, doi:10.1002/grl.50590.

Melgar, D., R. M. Allen, S. Riquelme, J. Geng, F. Bravo, J. C. Baez, H. Parra, S. Barrientos, P. Fang, and Y. Bock (2016), Local tsunami warnings: Perspectives from recent large events, *Geophys. Res. Lett*, *43*, 1109–1117, doi:10.1002/2015GL067100.

O'Toole, T. B., A. P. Valentine, and J. H. Woodhouse (2012), Centroid-moment tensor inversions using high-rate GPS waveforms, *Geophys. J. Int.*, *191*(1), 257–270.

O'Toole, T. B., A. P. Valentine, and J. H. Woodhouse (2013), Earthquake source parameters from GPS-measured static displacements with potential for real-time application, *Geophys. Res. Lett.*, *40*, 60–65, doi:10.1029/2012GL054209.

Ohta, Y., et al. (2012), Quasi real-time fault model estimation for near-field tsunami forecasting based on RTK-GPS analysis: Application to the 2011 Tohoku-Oki earthquake (M_w 9.0), *J. Geophys. Res.*, *117*, L12302, doi:10.1029/2011JB008750.

Okada, Y. (1985), Surface deformation due to shear and tensile faults in a half-space, *Bull. Seismol. Soc. Am.*, *75*(4), 1135–1154.

Saastamoinen, J. (1972), Atmospheric correction for the troposphere and stratosphere in radio ranging satellites, *use Artif. Satell. Geod.*, 247–251.

Schurr, B., G. Asch, S. Hainzl, J. Bedford, A. Hoechner, M. Palo, R. Wang, M. Moreno, M. Bartsch, and Y. Zhang (2014), Gradual unlocking of plate boundary controlled initiation of the 2014 Iquique earthquake, *Nature*, *512*, 299–302.

Sobolev, S. V., A. Y. Babeyko, R. Wang, R. Galas, M. Rothacher, D. Sein, J. Schröter, J. Lauterjung, and C. Subarya (2006), Towards real-time tsunami amplitude prediction, *Eos Trans. AGU*, *87*(37), 374–378, doi:10.1029/2006EO370003.

Sobolev, S. V., A. Y. Babeyko, R. Wang, A. Hoechner, R. Galas, M. Rothacher, D. V. Sein, J. Schröter, J. Lauterjung, and C. Subarya (2007), Tsunami early warning using GPS-Shield arrays, *J. Geophys. Res.*, *112*, B08415, doi:10.1029/2006JB004640.

Song, Y. T. (2007), Detecting tsunami genesis and scales directly from coastal GPS stations, *Geophys. Res. Lett.*, *34*, L19602, doi:10.1029/2007GL031681.

Tu, R., R. Wang, M. Ge, T. R. Walter, M. Ramatschi, C. Milkereit, D. Bindi, and T. Dahm (2013), Cost-effective monitoring of ground motion related to earthquakes, landslides, or volcanic activity by joint use of a single-frequency GPS and a MEMS accelerometer, *Geophys. Res. Lett.*, *40*, 3825–3829, doi:10.1002/grl.50653.

Wang, R., F. L. Martín, and F. Roth (2003), Computation of deformation induced by earthquakes in a multi-layered elastic crust—FORTRAN programs EDGRN/EDCMP, *Comput. Geosci.*, *29*(2), 195–207.